ORGANOMETALLICS

Article

pubs.acs.org/Organometallics

Partially Shielded $Fe(CO)_3$ Rotors: Syntheses, Structures, and Dynamic Properties of Complexes with Doubly *trans* Spanning Diphosphines, *trans*-$Fe(CO)_3(PhP((CH_2)_n)_2PPh)$

Esther Steigleder,[†] Takanori Shima,[†] Georgette M. Lang,[‡] Andreas Ehnbom,[‡] Frank Hampel,[†] and John A. Gladysz*[,†,‡]

[†]Institut für Organische Chemie and Interdisciplinary Center for Molecular Materials, Friedrich-Alexander-Universität Erlangen-Nürnberg, Henkestraße 42, 91054 Erlangen, Germany

[‡]Department of Chemistry, Texas A&M University, P.O. Box 30012, College Station, Texas 77843-3012, United States

Supporting Information

ABSTRACT: Reactions of $Fe(CO)_3(\eta^4$-benzylideneacetone) and $PhP((CH_2)_mCH{=}CH_2)_2$ (m = **a**, 4; **b**, 5; **c**, 6) give *trans*-$Fe(CO)_3(PhP((CH_2)_mCH{=}CH_2)_2)_2$ (**2a−c**, 28−70%), which are treated with Grubbs' catalyst (15 mol %; refluxing CH_2Cl_2). NMR analyses of the crude *inter*ligand metathesis products *trans*-$Fe(CO)_3(PhP((CH_2)_mCH{=}CH(CH_2)_m)_2PPh)$ (**3a−c**, 30−31%) suggest Z/E C=C mixtures and/or byproducts from *intra*ligand metathesis or oligomers. Subsequent hydrogenations (5 bar/cat. $Rh(Cl)(PPh_3)_3$ or PtO_2) afford *trans*-$Fe(CO)_3(PhP((CH_2)_n)_2PPh)$ (**4a−c**, 69−77%; $n = 2m + 2$, *synperiplanar* phenyl groups), which density functional theory calculations show to be more stable than isomers derived from other metathesis modes. Crystallizations give (E,E)-**3a** and **4b**, the X-ray structures of which are determined and analyzed. Variable-temperature $^{13}C\{^1H\}$ NMR experiments show that rotation of the $Fe(CO)_3$ moiety in **4b** is rapid on the NMR time scale (RT to 0 °C; $\Delta G^{\ddagger}_{273\ K} \leq 12.8$ kcal/mol), but that in **4a** is not (RT to 105 °C; $\Delta G^{\ddagger}_{378\ K} \geq 17.9$ kcal/mol). These data indicate rotational barriers lower than those in analogues in which three methylene chains connect the phosphorus atoms, *trans*-$Fe(CO)_3(P((CH_2)_n)_3P)$.

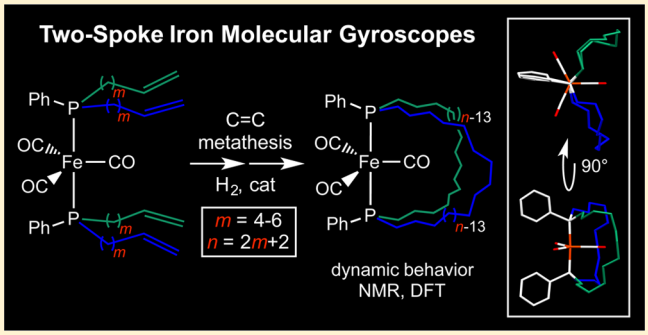

INTRODUCTION

The intersection of alkene metathesis and inorganic or organometallic synthesis has proved to be a rich area, allowing targeted approaches to a variety of complex metal-containing molecules.[1,2] We evolved initial interests in metallomacrocycle and metallamacrocycle syntheses (**I** and **II** in Scheme 1)[3,4] into a program involving gyroscope-like complexes of the general type **IIIa**.[5−11] These are distinguished by three methylene chains that span two *trans*-phosphorus donor atoms and are assembled by alkene metathesis/hydrogenation sequences. Some of the most interesting and intensively studied species have trigonal planar iron carbonyl cores or "rotators" ($Fe(CO)_3$, $Fe(CO)_2(NO)^+$, $Fe(CO)(NO)(X)$)[5] within the *di*bridgehead *di*phosphine "stators". Many crystal structures and barriers to $Fe(CO)(L)(L')$ rotation have been determined.

The interpretation of the rotational barriers has required a variety of supporting synthetic and physical studies. For example, analogous dibridgehead di*arsine* complexes have been prepared (**IIIb**).[12] Their distinctly lower barriers have been analyzed in the context of the longer iron−arsenic versus iron−phosphorus bonds and a resulting increase in vertical (top/bottom) free van der Waals space within the cage-like assembly.

As such, another goal became the synthesis of related trigonal bipyramidal complexes with *two* instead of three *trans* spanning methylene chains. These would have fewer impediments in a horizontal dimension to rotator rotation. Also, their lower symmetries can simplify the determination of activation parameters by variable-temperature NMR. Accordingly, in this paper, we describe the syntheses, structures, and dynamic properties of a series of iron tricarbonyl bis(*phenyl*dialkylphosphine) complexes of the formula *trans*-$Fe(CO)_3(PhP((CH_2)_n)_2PPh)$ (n = 10, 12, 14). A number of characteristics are carefully compared to those of related species **IIIa**, affording new insights regarding the various factors contributing to $Fe(CO)(L)(L')$ rotational barriers.

RESULTS

Syntheses of Title Complexes. The monophosphine ligands needed for the precursor iron complexes, $PhP((CH_2)_mCH{=}CH_2)_2$

Received: May 8, 2017

 © XXXX American Chemical Society

DOI: 10.1021/acs.organomet.7b00330
Organometallics XXXX, XXX, XXX−XXX

Scheme 1. Typical Metal-Containing Macrocycles Constructed via Alkene Metathesis (i = Grubbs' Catalyst; ii = H_2, Hydrogenation Catalyst)

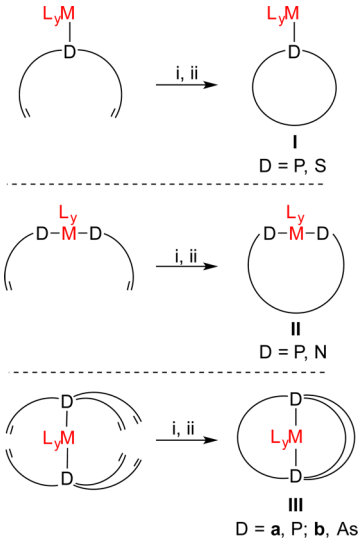

(**1**; m = **a**, 4; **b**, 5; **c**, 6), were accessed by one of two methods. The first, a published procedure,[3a,c] involved the initial addition of $PhPH_2$ and n-BuLi (2.0 equiv) to give the dilithiated phosphorus nucleophile $PhPLi_2$. Subsequent reactions with α,ω-bromoalkenes $Br(CH_2)_mCH{=}CH_2$ (2.0 equiv) afforded **1a–c** in 51–59% yields. The second, new to this work, involved initial conversions of $Br(CH_2)_mCH{=}CH_2$ to the corresponding Grignard reagents, followed by additions of $PhPCl_2$ (0.5 equiv). Workups gave **1a–c** in 78–90% yields.

The corresponding bis(phosphine) iron tricarbonyl complexes were prepared analogously to the similar precursors to **IIIa** (Scheme 1).[5] As shown in Scheme 2, the substitution

Scheme 2. Syntheses of the Title Complexes

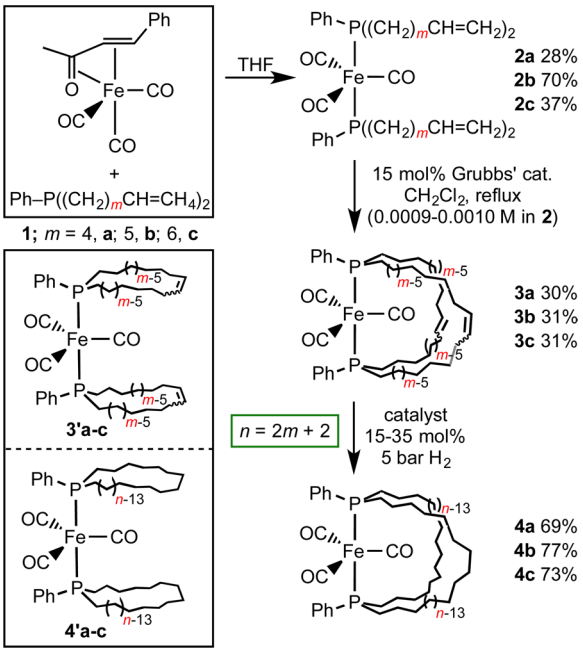

labile precursor $Fe(CO)_3(\eta^4$-benzylideneacetone)[13] and **1a–c** (2.0 equiv) were combined in THF. Workups gave the expected adducts *trans*-$Fe(CO)_3(PhP((CH_2)_mCH{=}CH_2)_2)_2$ (**2a–c**) as yellow-brown oils in 28–70% yields. These and all other isomerically homogeneous new complexes described below were characterized by IR and NMR (^1H, $^{13}C\{^1H\}$, $^{31}P\{^1H\}$) spectroscopy, and often by mass spectrometry and microanalyses, as summarized in the Experimental Section. Key NMR data are presented in Table 1.

Next, dilute CH_2Cl_2 solutions of **2a–c** (0.0009–0.0010 M) were treated with Grubbs' first generation catalyst (7.5 mol %, or 3.75%/new C=C linkage). The samples were stirred at 45 °C, and aliquots were monitored by ^1H and $^{31}P\{^1H\}$ NMR. The data were consistent with the formation of the target *inter*ligand metathesis products *trans*-$Fe(CO)_3(PhP((CH_2)_mCH{=}CH{-}(CH_2)_m)_2PPh)$ (**3a–c**). However, a second catalyst charge (7.5 mol %) was necessary for the complete consumption of all terminal alkene moieties. Workups gave crude **3a–c** in 30–31% yields.

The NMR data suggested that **3a–c** were mixtures of C=C geometric isomers (e.g., *EE*, *EZ*, *ZZ*). The ^{31}P NMR spectra showed more than three signals, suggesting the presence of oligomers or other types of isomers, one possibility being **3′a–c** (Scheme 2), derived from *intra*ligand metathesis. In any case, **3a–c** were hydrogenated (5 bar, 15 h) using either Wilkinson's catalyst or PtO_2. Chromatographic workups gave the title complexes *trans*-$Fe(CO)_3(PhP((CH_2)_n)_2PPh)$ (**4a–c**; $n = 2m + 2$) as white-yellow gums or waxes in 69–77% yields (21–24% from **2a–c**). These feature 13-, 15-, and 17-membered macrocycles, respectively. No significant amounts of the isomeric species *trans*-$Fe(CO)_3(PhP(CH_2)_n)_2$ (**4′a–c**; Scheme 2) were detected. Relevant to an analysis below, note that conformations in which the phenyl groups are *anticlinal* (Ph–P–P–Ph dihedral angle 120°, as opposed to the 0° depicted) are available to **4′a–c** but not **4a–c**.

Several NMR properties of **4a–c** (see Table 1) deserve emphasis. First, the $PCH_2CH_2CH_2$ $^{13}C\{^1H\}$ signals could be assigned by analogy to those of iron tricarbonyl complexes of the type **IIIa**. The PCH_2 and the $PCH_2CH_2CH_2$ signals were either virtual triplets[14] or apparent (second-order) doublets of doublets with comparable coupling constants. The PCH_2CH_2 signals did not exhibit detectable phosphorus couplings. The PC_6H_5 $^{13}C\{^1H\}$ signals of **4a–c** as well as **2a–c** were assigned by standard protocols.[15] The *o*-Ph and *m*-Ph signals were virtual triplets.[14] However, some *i*-Ph signals were virtual triplets, and others were apparent doublets of doublets. The *p*-Ph signals did not show detectable phosphorus couplings.

The CO $^{13}C\{^1H\}$ NMR signals of **4a–c** were phosphorus coupled triplets with $^2J_{CP}$ values ranging from 26.8 to 29.1 Hz. Depending on the macrocycle size, either one triplet or two (ca. 2:1 area ratio) were observed. These data are interpreted in the context of variable-temperature NMR experiments below. The noncyclized complexes **2a–c** always exhibited a single CO signal (t, $^2J_{CP}$ = 28.5–28.7 Hz), as would the isomers **4′a–c**.

Molecular Structures. Attempts were made to crystallize the preceding samples. These were successful in the cases of **3a** and **4b**, which have 13- and 15-membered macrocycles. With the former, crystals of the *trans,trans* C=C isomer (*E,E*)-**3a** were obtained. In other alkene metatheses of complexes with *trans*-$H_2C{=}CH(CH_2)_4P$-M-$P(CH_2)_4CH{=}CH_2$ linkages, marked preferences for *trans* (*E*) isomers have been observed,[3b,c,5a,b,12] and rationales have been suggested.[5b]

DOI: 10.1021/acs.organomet.7b00330
Organometallics XXXX, XXX, XXX–XXX

Table 1. Selected $^{31}P\{^1H\}$ and $^{13}C\{^1H\}$ NMR Data for 2a−c and 4a−c[a]

complex	$^{31}P\{^1H\}$ (δ/ppm)	$^{13}C\{^1H\}$ (δ/ppm)							
		CO [$^2J_{PC}$, Hz]	P<u>C</u>H$_2$ [$^1J_{PC}$, Hz]	PCH$_2$<u>C</u>H$_2$	PCH$_2$CH$_2$<u>C</u>H$_2$ [$^3J_{PC}$, Hz]	*i*-Ph [$^1J_{PC}$, Hz]	*o*-Ph [$^2J_{PC}$, Hz]	*p*-Ph	*m*-Ph [$^4J_{PC}$, Hz]
2a[b]	70.1	215.6 [28.6][c]	33.0 [15.3], [13.3][d]	24.1	30.6 [6.6][e]	*f*	131.9 [4.6][e]	130.0	128.7 [4.3][e]
2b	69.0	215.6 [28.6][c]	33.1 [15.4], [13.5][d]	24.4	30.8 [6.6][e]	136.4 [21.5], [17.4][d]	131.9 [4.7][e]	130.2	128.7 [4.4][e]
2c	69.8	215.7 [28.5][c]	33.2 [15.9], [12.5][d]	24.6	31.4 [6.6][e]	136.5 [21.4], [17.6][d]	131.8 [4.6][e]	129.9	128.7 [4.5][e]
4a	78.0	216.5[g] [28.5];[c] 215.1[g] [26.8][c]	32.4 [15.5], [13.6][d]	24.1	29.0 [6.2][e]	136.5 [20.3], [17.3][d]	132.1 [5.1][e]	130.1	128.8 [4.5][e]
4b	72.6	215.4 [29.1][c]	34.0 [15.7], [13.7][d]	23.2	29.7 [7.3][e]	136.8 [21.0], [17.1][d]	132.1 [5.0][e]	130.0	128.8 [4.6][e]
4c	72.0	214.1 [28.8][c]	34.0 [13.6][e]	24.7	31.1 [6.9][e]	136.9 [21.0], [16.9][d]	132.2 [4.6][e]	130.2	128.9 [4.2][e]

[a]NMR spectra were recorded on a 400 MHz instrument in C_6D_6. Signals for which no *J* values are indicated are singlets. [b]The data for **2a** are taken from the NMR spectra in the Supporting Information, for which some couplings were better resolved. [c]These *J* values are for triplets. [d]These *J* values are for apparent doublet of doublets. [e]These *J* values are for virtual triplets. [f]The expected signal was not observed. [g]The upfield signal is more intense (ca. 2:1 ratio per Figure 4).

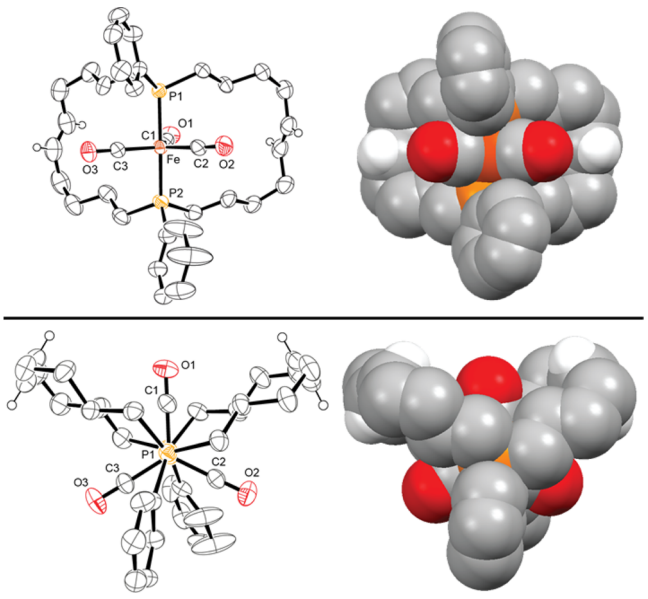

Figure 1. Thermal ellipsoid (left) and space-filling (right) representations of the molecular structure of (*E*,*E*)-**3a**; views with the P−Fe−P axis in the plane (top) and perpendicular to the plane (bottom) of the paper.

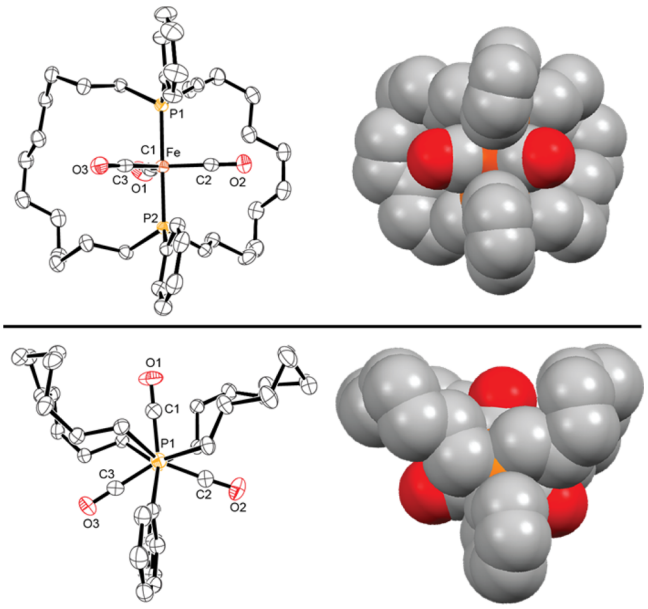

Figure 2. Thermal ellipsoid (left) and space-filling (right) representations of the molecular structure of **4b**; views with the P−Fe−P axis in the plane (top) and perpendicular to the plane (bottom) of the paper.

The crystal structures of (*E*,*E*)-**3a** and **4b** were determined as outlined in Table S1 (Supporting Information) and the Experimental Section. Thermal ellipsoid plots and space-filling models are depicted in Figures 1 and 2. Key metrical parameters are listed in Table 2. The C_{ipso}−P1−P2−C_{ipso} torsion angles of (*E*,*E*)-**3a** and **4b** provide measures of the relative dispositions of the phenyl rings. The values are close to zero (−36.22 and 3.67°, respectively), indicative of *synperiplanar* orientations. The Fe−P−C_{ipso}−C_{ortho} torsion angles are also close to zero (Table 2), indicating roughly parallel dispositions of the phenyl rings and P−Fe−P axes.

Figure 3 shows the unit cells of (*E*,*E*)-**3a** and **4b**, each of which contains four molecules. In all neutral trigonal bipyramidal complexes of the type **IIIa** that have been crystallized to date, the P−M−P axes are parallel (ML_y = Fe(CO)$_3$,[5a,b,12] Os(CO)$_3$,[10a] Fe(CO)(NO)(X)[5c]).[16] In contrast, the P−Fe−P axes in crystalline (*E*,*E*)-**3a** and **4b** clearly orient in more than one direction. In the latter, there are two sets of molecules with parallel axes (such that an axis from one set would not be parallel to an axis from the other set). Thus, least-squares planes are defined using six atoms from *two* P−Fe−P axes from each set (planes defined by only three nearly collinear experimental points have large error limits). These intersect at an 89° angle, consistent with the near perpendicular orientation that is visually apparent in Figure 3 (bottom). With (*E*,*E*)-**3a**, there are four such sets, and the angles involving all six possible combinations are given in Table 2 (48−82°).

The radii of the Fe(CO)$_3$ rotators of (*E*,*E*)-**3a** and **4b** were estimated by taking the average <u>Fe</u>C<u>O</u> distances (2.92−2.93 Å; Table 2) and adding the van der Waals radius of an oxygen atom (1.52 Å;[17] sums = 4.44−4.45 Å). The average distances from the iron atoms to the two carbon atoms of each macrocycle closest to the planes of the Fe(CO)$_3$ rotators were also calculated (Table 2), and the van der Waals radius of a carbon atom (1.70 Å)[17] was *subtracted*. This can be viewed as one measure of the horizontal free van der Waals space or "clearance" within the

DOI: 10.1021/acs.organomet.7b00330
Organometallics XXXX, XXX, XXX−XXX

Table 2. Key Distances (Å) and Angles (deg) for Crystalline (*E*,*E*)-3a and 4b

	(*E*,*E*)-**3a**	**4b**
distances		
Fe−P1/Fe−P2	2.2153(10)/2.2239(10)	2.2097(7)/2.2108(7)
P1−P2	4.4543(20)	4.4205(14)
Fe−C1/Fe−C2/Fe−C3	1.761(4)/1.760(4)/1.772(4)	1.766(3)/1.770(2)/1.777(2)
C1−O1/C2−O2/C3−O3	1.163(4)/1.158(4)/1.162(4)	1.156(3)/1.163(3)/1.156(3)
avg FeCO	2.924	2.929
avg FeCO + O vdW[a]	4.44	4.45
Fe−C_d[b]	5.385/5.407/5.540/5.525	6.047/5.849/6.011/5.936
avg Fe−C_d	5.464	5.961
avg Fe−C_d − C vdW[a]	3.76	4.26
Fe−$C_{neighbor}$[c]	5.175	5.503
Fe−$C_{neighbor}$ − C vdW[a]	3.48	3.80
bond angles		
P1−Fe−P2	171.82(4)	176.48(3)
Fe−C1−O1/Fe−C2−O2/Fe−C3−O3	178.2(3)/178.9(4)/176.9(3)	179.3(2)/176.9(2)/179.1(2)
P1−Fe−C1/P1−Fe−C2/P1−Fe−C3	85.34(11)/91.42(12)/89.29(12)	89.35(8)/91.63(8)/89.94(7)
P2−Fe−C1/P2−Fe−C2/P2−Fe−C3	86.68(11)/91.42(12)/96.08(12)	89.47(8)/91.87(8)/88.10(7)
Fe−P1−C_i/Fe−P2−C_i[d]	118.24(11)/120.69(11)	116.37(8)/116.04(7)
Fe−P1−C_a/Fe−P2−C_a[e]	114.26(12)/114.88(11)/ 114.10(14)/113.46(12)	116.14(7)/116.13(8) 116.38(8)/116.30(8)
torsion and other angles		
C_i−P1−P2−C_i[d]	−36.22	3.67
Fe−P1−C_i−C_o[d,f]	17.0(3)	4.6(2)
Fe−P2−C_i−C_o[d,f]	−20.9(5)	−16.6(2)
[P−Fe−P + P−Fe−P]/[P′−Fe′−P′ + P′−Fe′−P′][g]	82.1/75.8/62.9/56.2/56.0/48.3	89

[a]vdW = van der Waals. [b]The subscript *d* (distal) denotes the two carbon atoms of each macrocycle that are closest to the plane of the rotator. For (*E*,*E*)-**3a**: C5a/C6a/C5b/C6b. For **4b**: C16/C17/C36/C37. [c]$C_{neighbor}$ denotes the closest atom (always carbon) of a neighboring molecule. For (*E*,*E*)-**3a**, C8A. For **4b**, C65, with C33 only slightly more distant (5.527 Å). [d]C_i denotes an *ipso* C_6H_5 carbon atom. [e]C_a denotes a macrocyclic carbon atom bound to a phosphorus atom. [f]C_o denotes an *ortho* C_6H_5 carbon atom. [g]Least-squares planes are defined using the six atoms of two P−Fe−P axes of all molecules with parallel axes in the lattice. These values represent the angles between all such planes.

macrocycles. In (*E*,*E*)-**3a**, this value is much shorter than the radius of the rotator (3.76 Å), whereas in **4b**, it is nearly comparable (4.26 Å).

The non-hydrogen atoms of neighboring molecules nearest to the iron atoms in (*E*,*E*)-**3a** and **4b** were identified, and the van der Waals radii of these nearby atoms were subtracted from the distances. As summarized in Table 2, these intermolecular "clearances" are significantly less than the radius of the rotators (3.48−3.80 Å vs 4.44−4.45 Å). Hence, there should be additional impediments to $Fe(CO)_3$ rotation in the solid state.

Dynamic Properties and Computations. The barriers to $Fe(CO)_3$ rotation in the title molecules were probed by variable-temperature $^{13}C\{^1H\}$ NMR. Various limiting situations were anticipated. In one, the macrocycles would be too small to allow $Fe(CO)_3$ rotation under any conditions. This would be evidenced by two CO ^{13}C signals in a ca. 2:1 area ratio at all accessible temperatures. In another, the macrocycles would be sufficiently large for facile $Fe(CO)_3$ rotation, even at very low temperatures. This would be evidenced by a single CO ^{13}C signal. In a more informative scenario, both limits could be observed depending upon temperature, and activation parameters could be calculated from signal coalescence or line shape data.

Complex **4a** features 13-membered macrocycles with 10 CH_2 groups, and variable-temperature $^{13}C\{^1H\}$ NMR spectra were recorded in toluene-d_8, as depicted in Figure 4. Although the signal/noise ratio was not optimal, two CO ^{13}C NMR signals (each phosphorus coupled triplets as noted above) were plainly visible at 25 °C. Spectra at higher temperatures showed no hint of any onset of coalescence, even at 105 °C (378 K). Application of the coalescence formula[18] allows the $\Delta G^{\ddagger}_{378\ K}$ value for $Fe(CO)_3$ rotation to be bounded as greater than 17.9 kcal/mol, as derived in the Supporting Information.

Complex **4b** features 15-membered macrocycles with 12 CH_2 groups, and variable-temperature $^{13}C\{^1H\}$ NMR spectra were recorded in CD_2Cl_2, as depicted Figure S1 (signal/noise similar to that in Figure 4) in the Supporting Information. As noted above, only one signal was observed at 25 °C. However, the results upon cooling were ambiguous. New signals seemed to appear below 0 °C, but there was not a clear-cut decoalescence, in part due to the signal/noise. Nonetheless, an upper limit on the rotational barrier could be estimated, as described below.

During the review phase of this paper, a referee inquired about the relative stabilities of isomers of the types **3**/**4** and **3′**/**4′** in Scheme 2 as well as variants of the former in which the phenyl groups are *antiperiplanar* as opposed to *synperiplanar* (**3″**/**4″**; vide infra). Hence, a computational investigation was conducted, focusing on the saturated systems **4**, **4′**, and **4″** to avoid the complication of multiple C═C isomers. With **4′**, conformations with *synperiplanar* and *anticlinal* phenyl groups were both examined. Density functional theory (DFT) calculations were carried out as described in the Experimental Section, and the relative energies found with one functional (CAM-B3LYP) are presented in Figure 5. Similar data were obtained with other functionals, as summarized in Table S2 (Supporting Information). The results were further validated by the excellent agreement of the computed structure of **4b** with the crystal structure (Figure S2). The trends evident in Figure 5 are analyzed below.

DOI: 10.1021/acs.organomet.7b00330
Organometallics XXXX, XXX, XXX−XXX

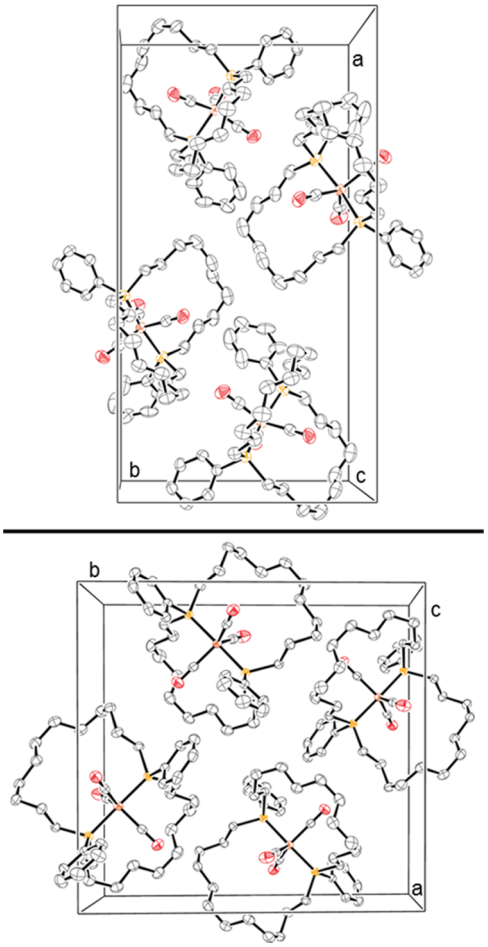

Figure 3. Unit cells of (*E*,*E*)-**3a** (top) and **4b** (bottom).

DISCUSSION

Syntheses. The lower symmetries of the title complexes **4a**−**c** versus the analogous gyroscope-like species **IIIa** (ML_y = $Fe(CO)_3$) carry subtle implications regarding their syntheses. Consider first the structure **VIII** in Scheme 3 (top), which represents a precursor to **IIIa**. As noted in previous papers,[5] the phosphorus atom substituents will prefer to be staggered relative to the carbonyl groups on iron. This preorganizes the reactants for three-fold *intra*molecular *inter*ligand ring-closing alkene metatheses. After the first *trans* spanning linkage is generated (**IX**), the remaining $(CH_2)_mCH{=}CH_2$ groups are locked into place for analogous couplings, which result in **X**. For simplicity, each cyclization in Scheme 3 incorporates a hydrogenation step.

Contrast this to the scenario with **2a**−**c**. As shown in Scheme 3 (bottom), two inequivalent conformations are now possible in which the phosphorus atom substituents are staggered relative to the carbonyl groups on iron, **XI** (idealized C_{2v} symmetry, *synperiplanar* phenyl groups) and **XIII** (C_2, *anticlinal* phenyl groups). With **XI**, after the first *trans* spanning linkage is generated (**XII**), the two remaining $(CH_2)_mCH{=}CH_2$ groups are locked into place for coupling to the product **IV** (**4a**−**c**) However, with **XIII**, only a single *trans* spanning linkage can readily be generated (**XIV**). To form a second, $(CH_2)_mCH{=}CH_2$ groups from different OC−Fe−CO interstices must couple. As can be seen in **XIV** and **XV**, a carbonyl ligand provides considerable interference. Furthermore, the product **XV** is not topologically equivalent to **IV** but is rather a distorted form of **V** (idealized C_s symmetry), a diastereomer of **IV** in which the two phenyl rings have an *antiperiplanar* arrangement. This corresponds to the structures **4″a**−**c** in Figure 5.

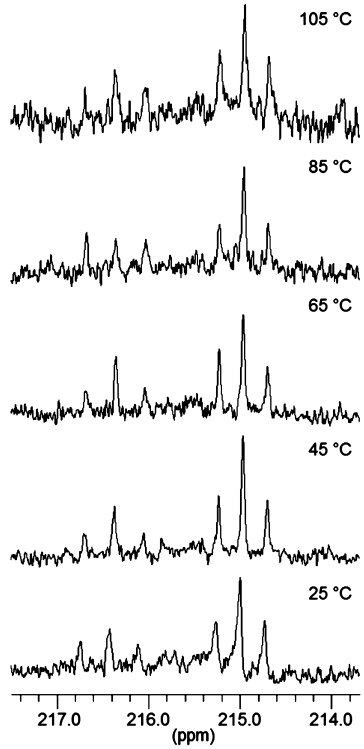

Figure 4. Partial $^{13}C\{^1H\}$ NMR spectra of **4a** in toluene-d_8 as a function of temperature.

Hence, *inter*molecular alkene metatheses, such as oligomerization, or *intra*ligand metatheses to give species of the type **4′a**−**c** should be able to better compete with reactants of the type **2a**−**c**. Accordingly, the yields of crude **3a**−**c** (30−31%) are low compared to those of analogues in which three methylene chains span the *trans* phosphorus atoms (60−81%).[5a,b] Alternatively, the overall yields after hydrogenation can be compared (21−24% vs 34−51%).

Alkene metatheses have also been carried out using square planar platinum complexes with *trans*-phosphine ligands **1a**−**c**, as shown in Scheme 4.[3c] With this coordination geometry, no conformation is possible that preorganizes the reactants for three-fold *inter*ligand metathesis. Accordingly, the yields of monoplatinum metathesis/hydrogenation products **6a**−**c** are low (5−38%). With **6c**, which has the largest macrocycles (17-membered), diastereomers with *synperiplanar* and *antiperiplanar* phenyl rings are both produced (31:7; cf. **IV** and **V** in Scheme 3). No products involving *intra*ligand metathesis have been detected. However, when the alkyl chains of the phosphines are reduced to two methylene groups, this becomes the exclusive reaction mode (86% isolated). Other experiments show that the larger pentafluorophenyl ligand constitutes an additional impediment to *inter*ligand metathesis.[6b,19]

Although this study was not designed to explore the reactivity of **2a**−**c** or **4a**−**c**, NMR tube experiments show that they can be protonated at iron with strong acids or one CO ligand displaced upon addition of NO^+ BF_4^-, affording tetrafluoroborate salts of the isosteric and isoelectronic $Fe(CO)_2(NO)^+$ species. Both types of reactions have abundant precedent with **IIIa** (ML_y = $Fe(CO)_3$) or their acyclic precursors.[5,20]

Physical Properties. As shown in Figures 1 and 2, crystalline (*E*,*E*)-**3a** and **4b** exhibit approximately staggered arrangements

DOI: 10.1021/acs.organomet.7b00330
Organometallics XXXX, XXX, XXX−XXX

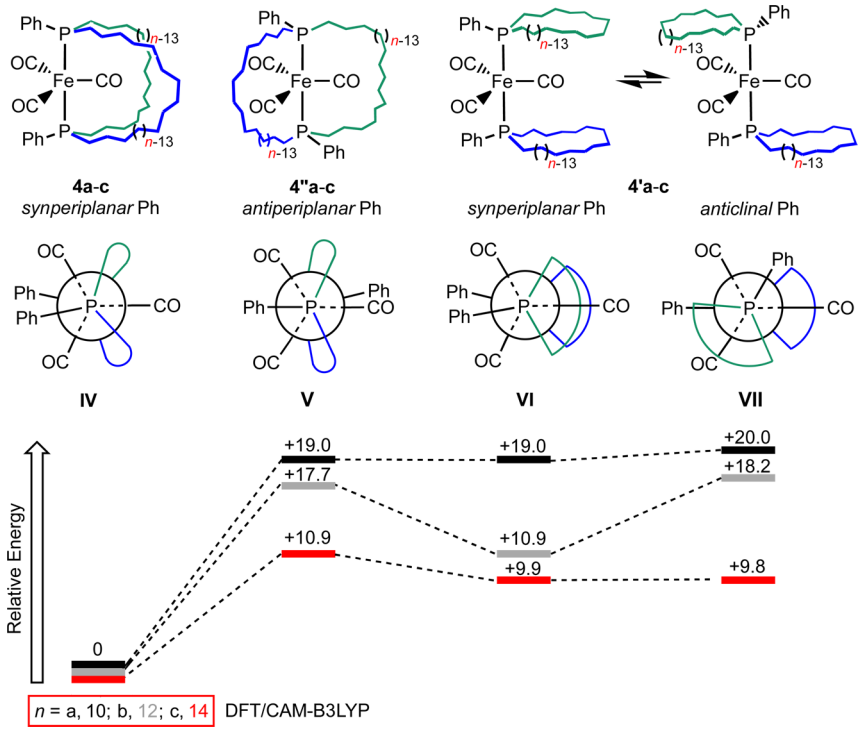

Figure 5. Relative energies (kcal/mol) of the isomers **4**, **4″**, **4′**$_{synperiplanar}$, and **4′**$_{anticlinal}$ as computed by DFT.

Scheme 3. Conformations of 2a−c (XI, XIII) and Implications for Alkene Metathesis/Hydrogenation Products

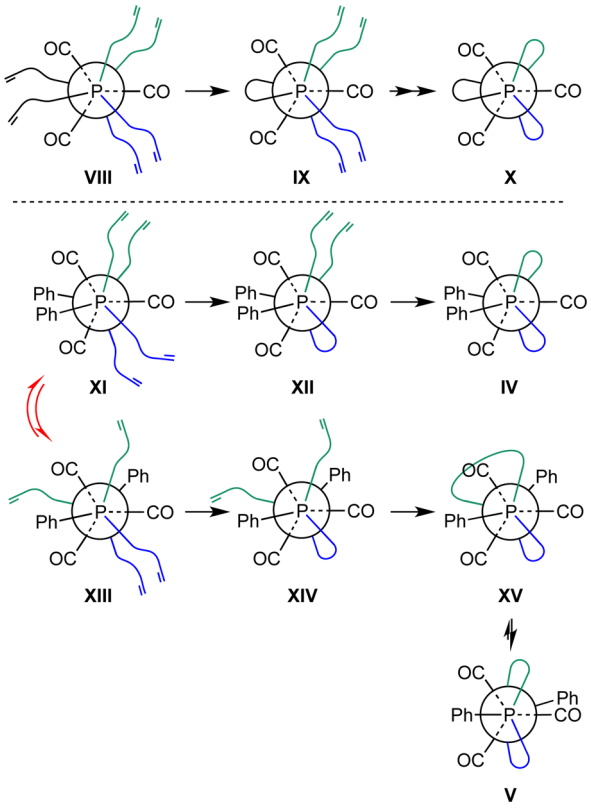

Scheme 4. Alkene Metathesis/Hydrogenation Sequences Using Square Planar Platinum Complexes with *trans*-Phosphine Ligands $P(CH_2)_mCH{=}CH_2$ (1a−c)

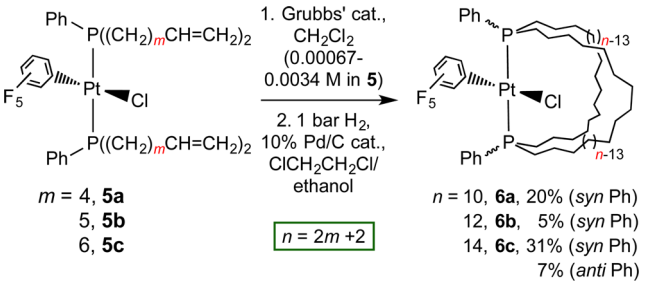

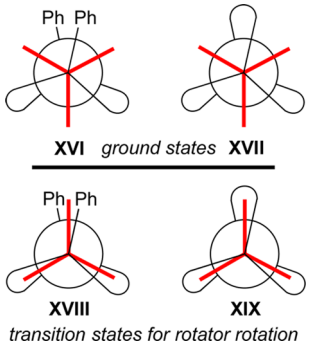

Figure 6. Conformational minima and maxima for the title complexes (left) and analogues with three *trans* spanning linkages (right).

of the phosphorus atom substituents and carbonyl ligands on iron, as posited for the precursors in Scheme 3. The crystal structure of the analogue of (*E*,*E*)-**3a** with *three* as opposed to two (*E*)-$(CH_2)_4CH{=}CH(CH_2)_4$ linkages spanning the *trans*-phosphorus atoms has also been determined (two different solvates).[5a,b]

In contrast, **4b** represents a new macrocycle size for crystallographically characterized $Fe(CO)_3$ adducts of *trans* spanning diphosphine ligands. However, the structure of the diarsine analogue with three $(CH_2)_{12}$ linkages has been determined.[12]

The dimensions of the 13- and 15-membered macrocycles in (*E*,*E*)-**3a** and **4b** are in the range of those found earlier in the

DOI: 10.1021/acs.organomet.7b00330
Organometallics XXXX, XXX, XXX−XXX

diphosphine or diarsine analogues with three identical linkages.[5,12] For example, as noted above, the distances from iron to the two carbon atoms of each macrocycle closest to the plane of the rotator are given in Table 2 (5.39−5.54 Å for (*E*,*E*)-**3a**; 5.85−6.05 Å for **4b**). The corresponding distances for the analogues with three identical linkages are 5.34−5.35 and 5.62−6.38 Å, respectively. Probably the average values (5.46 vs 5.34 Å and 5.96 vs 5.94 Å) best reflect the typical horizontal extensions of the macrocycles in solution.

All of the iron complexes described in this paper, as well as **IIIa**,**b** with L_yM = $Fe(CO)_3$, $Fe(CO)_2(NO)^+$, or $Fe(CO)(NO)(X)$, possess three-fold barriers to $Fe(CO)(L')(L'')$ rotation—that is, three degenerate minima and maxima over the course of a 360° rotation.[21] These are depicted in Figure 6, with **XVI** and **XVIII** representing **3a**−**c**/**4a**−**c** and **XVII** and **XIX** representing **IIIa**,**b**. The maxima feature three-fold eclipsing interactions of the phosphorus substituents and iron carbonyl ligands. With **IIIa**,**b**, all three carbonyl ligands must simultaneously pass through the restricted space associated with the interior of the macrocycles (**XIX**). With the title compounds, only two carbonyl ligands must so transit (**XVIII**). Hence, given that macrocycles of the same sizes have roughly the same dimensions (vide supra), somewhat lower rotational barriers would be expected with **XVIII**.

This expectation is fulfilled, albeit with the proviso that the isosteric and isoelectronic rotator $Fe(CO)_2(NO)^+$ has been used as a surrogate for $Fe(CO)_3$ in complexes of the type **III**. This desymmetrization is required in order for two sets of $P(CH_2)_{n/2}$ ^{13}C NMR signals to be observed. Thus, variable-temperature $^{13}C\{^1H\}$ NMR spectra of *trans*-$[Fe(CO)_2(NO)(P((CH_2)_{12})_3P)]^+$ BF_4^- (three 15-membered macrocycles) exhibit two sets of $P(CH_2)_6$ signals at room temperature but only one at 100 °C (typical T_{coal} = 70 °C).[5b] The data allow $\Delta G^{\ddagger}_T$ values of 19.0 kcal/mol (378 K), 16.7 kcal/mol (298 K), or 16.1 kcal/mol (273 K) to be calculated. In contrast, **4b** gives one set of $Fe(CO)_3$ ^{13}C NMR signals at room temperature, and per Figure S1, T_{coal} is likely less than 0 °C. If one approximates the $\Delta\nu$ of the two ^{13}CO signals as the same as **4a** and assumes a T_{coal} of 0 °C,[22] an upper limit of 12.8 kcal/mol is obtained for the $\Delta G^{\ddagger}_{273\ K}$ value, as illustrated in the Supporting Information. This is several kcal/mol lower than that of the analogous complex of the type **IIIa**.

This limit can also be compared to the barrier for $Fe(CO)_2(NO)^+$ rotation in *trans*-$[Fe(CO)_2(NO)(P((CH_2)_{14})_3P)]^+$ BF_4^- (three 17-membered macrocycles), which has a $\Delta G^{\ddagger}_{273\ K}$ value of 11.3 kcal/mol. We therefore suggest that the barriers to rotator rotation in **4a**−**c** are comparable to those in homologous complexes **IIIa** with two additional methylene groups in each macrocycle. In the case of **4a** (two 13-membered macrocycles), a lower limit of 17.9 kcal/mol for the $\Delta G^{\ddagger}_{378\ K}$ value can be derived from Figure 4 without any chemical shift assumptions (Supporting Information). However, this affords little insight, as no evidence has been obtained to date that a CO ligand can pass through a 13-membered macrocycle in any complex of the types **IIIa**,**b**.

Finally, we return to Figure 5 and the energies of the two isomers derived from *inter*ligand metathesis, **4a**−**c** and **4″a**−**c**. The latter are computed to be much less stable, but the difference is greatest for **4a**/**4″a** (19.0 kcal/mol), which have the shortest methylene chains and 13-membered macrocycles. With **4c**/**4″c**, which have 17-membered macrocycles, the difference is nearly cut in half (10.9 kcal/mol). Indeed, considering the steric interactions en route to **4″a**−**c** outlined in Scheme 3, longer methylene chains should afford lower activation barriers and less strained products. Accordingly, for the platinum complexes in Scheme 4, isomers with *antiperiplanar* phenyl groups did form (as minor products) in the case of 17-membered macrocycles.

Interestingly, both conformers of **4′a**−**c** are also much less stable than **4a**−**c**. The difference is marked for the smaller 13-membered macrocycles (**4′a**, 20.0−19.0 kcal/mol), suggesting greater ring strain as compared that for **4a**, in which the macrocycles are two atoms larger. In the conformers of **4′c**, the energy differences versus that of **4c** are nearly halved (9.9−9.8 kcal/mol). Although the selectivities in the metathesis reactions in Scheme 2 remain a function of the corresponding alkenes, one would expect stability trends analogous to those in Figure 5 for the more stable C═C isomers. Hence, the high selectivity for **4a**−**c** as opposed to that of other isomeric monoiron products tracks the relative thermodynamic stabilities.[23]

■ CONCLUSION

Iron tricarbonyl complexes with doubly *trans* spanning diphosphine ligands of the formula $PhP((CH_2)_n)_2PPh$ (n = 10, 12, 14) are easily synthesized by metathesis/hydrogenation sequences from precursors with *trans*-$PhP((CH_2)_mCH{=}CH_2)_2$ ligands (m = 4, 5, 6). However, the yields are somewhat lower than for those of analogous complexes with triply *trans* spanning $P((CH_2)_n)_3P$ ligands, and rationales for increased amounts of byproducts have been presented. The doubly bridged complexes feature lower $Fe(CO)_3$ rotational barriers, as only two, as opposed to three, CO ligands must pass through macrocycles during the transition state. While these findings may not be highly surprising, they provide welcome confirmation of the physical models that have been proposed to govern dynamic behavior. Other approaches to reducing rotational barriers in *trans*-diphosphine complexes, in which multiple methylene chains connect the phosphorus atoms, will be described in the near future.

■ EXPERIMENTAL SECTION

General. Reactions were carried out under dry N_2 except for hydrogenations. Chemicals were treated as follows: THF and hexanes, distilled from Na/benzophenone; CH_2Cl_2, distilled from CaH_2; MeOH, distilled by rotary evaporation; $Br(CH_2)_4CH{=}CH_2$ (97%, Acros), $Br(CH_2)_5CH{=}CH_2$ (96%, Acros), $Br(CH_2)_6CH{=}CH_2$ (90%, Fluka), *n*-BuLi (2.5 M in hexanes, Acros), 1,2-dibromoethane (99%, Acros), $PhPCl_2$ (98%, Fluka), $PhPH_2$ (98%, Aldrich), Mg powder (99%, Fluka), NH_4Cl (Fluka), neutral alumina 507 C (Fluka), PtO_2 (83% Pt, Acros), $Rh(Cl)(PPh_3)_3$ (97%, Lancaster), and Grubbs' first generation catalyst $Ru({=}CHPh)(PCy_3)_2(Cl)_2$ (Aldrich), used as received. NMR spectra were recorded on standard FT 400 MHz instruments at ambient probe temperatures unless noted, with solvents used as received and referenced as follows (δ, ppm): ^1H, residual internal $CHCl_3$ (7.24) or C_6D_5H (7.15); ^{13}C, internal $CDCl_3$ (77.0) or C_6D_6 (128.0); $^{31}P\{^1H\}$ NMR, internal H_3PO_4 capillary (δ 0.00). IR and MS spectra were recorded on ASI React-IR 1000 and Micromass Zabspec instruments, respectively.

$PhP((CH_2)_4CH{=}CH_2)_2$ (1a). A. A Schlenk flask was charged with Mg powder (0.9539 g, 39.25 mmol), THF (40 mL), and 1,2-dibromoethane (0.2 g, 0.1 mL, 1.2 mmol) and cooled to 0 °C. Then, $Br(CH_2)_4CH{=}CH_2$ (4.00 g, 3.29 mL, 24.5 mmol) was added dropwise with stirring, and the cold bath was removed. After 2 h, the mixture was cooled to 0 °C, and $PhPCl_2$ (2.20 g, 1.67 mL, 12.3 mmol) was added over 5 min. After 2 h, saturated aqueous NH_4Cl (30 mL) was added. The aqueous phase was removed by syringe. The organic phase was removed by oil pump vacuum. The residue was extracted with CH_2Cl_2. The extracts were filtered through a plug of neutral alumina (2 × 2 cm). The

DOI: 10.1021/acs.organomet.7b00330
Organometallics XXXX, XXX, XXX−XXX

solvent was removed from the combined filtrates by oil pump vacuum to give **1a** as a colorless oil (2.64 g, 9.62 mmol, 78%). **B.**[24] A Schlenk flask was charged with $PhPH_2$ (1.028 g, 9.337 mmol) and THF (40 mL) and cooled to 0 °C. Then, *n*-BuLi (2.5 M in hexanes, 7.5 mL, 18.70 mmol) was added dropwise with stirring over 15 min. The colorless solution turned first orange and then bright yellow and became cloudy. After 10 min, $Br(CH_2)_4CH{=}CH_2$ (3.05 g, 2.50 mL, 18.7 mmol) was added. The cold bath was removed. After 4 h, the solvent was removed by oil pump vacuum. Vacuum distillation gave **1a** as a colorless oil (1.38 g, 5.01 mmol, 54%). NMR ($CDCl_3$, δ in ppm): ^1H (400 MHz) 7.57−7.46 (m, 2H, Ph), 7.40−7.29 (m, 3H, Ph), 5.79 (tdd, $^3J_{HH}$ = 6.7 Hz, $^3J_{HHcis}$ = 10.2 Hz, $^3J_{HHtrans}$ = 16.9 Hz, 2H, C*H*=), 5.06−4.87 (m, 4H, =CH_2), 2.10−1.96 (m, 4H, CH_2), 1.80−1.54 (m, 4H, CH_2), 1.54−1.28 (m, 8H, CH_2); $^{13}C\{^1H\}$ (100 MHz)[15] 138.9 (d, $^1J_{CP}$ = 15.2 Hz, *i*-Ph), 138.6 (s, CH=), 132.2 (d, $^2J_{CP}$ = 18.6 Hz, *o*-Ph), 128.5 (s, *p*-Ph), 128.2 (d, $^3J_{CP}$ = 6.8 Hz, *m*-Ph), 114.3 (s, =CH_2), 33.3 (s, CH_2), 30.4 (d, $^3J_{CP}$ = 11.6 Hz, CH_2), 28.1 (d, J_{CP} = 11.3 Hz, CH_2), 25.4 (d, $^1J_{CP}$ = 13.9 Hz, PCH_2);[25] $^{31}P\{^1H\}$ (162 MHz) −23.7 (s).

$PhP((CH_2)_5CH{=}CH_2)_2$ (1b). A. Mg powder (0.5490 g, 22.59 mmol), THF (30 mL), 1,2-dibromoethane (0.2 g, 0.1 mL, 1.2 mmol), $Br(CH_2)_5CH{=}CH_2$ (2.50 g, 2.15 mL, 14.1 mmol), $PhPCl_2$ (1.26 g, 0.96 mL, 7.06 mmol), and saturated aqueous NH_4Cl (25 mL) were combined in a procedure analogous to **A** for **1a**. An identical workup gave **1b** as a colorless oil (1.70 g, 5.61 mmol, 79%). **B.**[24] $PhPH_2$ (1.028 g, 9.337 mmol), THF (40 mL), *n*-BuLi (2.5 M in hexanes, 7.50 mL, 18.7 mmol), and $Br(CH_2)_5CH{=}CH_2$ (3.31 g, 2.85 mL, 18.7 mmol) were combined in a procedure analogous to **B** for **1a**. An identical workup gave **1b** as a colorless oil (1.44 g, 4.76 mmol, 51%). NMR ($CDCl_3$, δ in ppm): ^1H (400 MHz) 7.50 (dt, J_{HH} = 1.8 Hz, J_{HH} = 7.4 Hz, 2H, Ph), 7.37−7.30 (m, 3H, Ph), 5.77 (tdd, $^3J_{HH}$ = 6.7 Hz, $^3J_{HHcis}$ = 10.2 Hz, $^3J_{HHtrans}$ = 16.9 Hz, 2H, C*H*=), 4.95−4.88 (m, 4H, =CH_2), 2.03−1.92 (m, 4H, CH_2), 1.73−1.60 (m, 4H, CH_2), 1.50−1.24 (m, 12H, CH_2); $^{13}C\{^1H\}$ (100 MHz)[15] 139.0 (d, $^1J_{CP}$ = 18.0 Hz, *i*-Ph), 138.9 (s, CH=), 132.3 (d, $^2J_{CP}$ = 18.5 Hz, *o*-Ph), 128.5 (s, *p*-Ph), 128.2 (d, $^3J_{CP}$ = 6.8 Hz, *m*-Ph), 114.2 (s, =CH_2), 33.6 (s, CH_2), 30.7 (d, J_{CP} = 11.5 Hz, CH_2), 28.5 (s, CH_2), 28.2 (d, J_{CP} = 11.1 Hz, CH_2), 25.8 (d, $^1J_{CP}$ = 13.7 Hz, PCH_2);[25] $^{31}P\{^1H\}$ (162 MHz) −23.4 (s).

$PhP((CH_2)_6CH{=}CH_2)_2$ (1c). A. Mg powder (0.7083 g, 29.14 mmol), THF (40 mL), 1,2-dibromoethane (0.2 g, 0.1 mL, 1.2 mmol), $Br(CH_2)_6CH{=}CH_2$ (3.99 g, 3.50 mL, 20.9 mmol), $PhPCl_2$ (1.86 g, 1.20 mL, 10.4 mmol), and saturated aqueous NH_4Cl (25 mL) were combined in a procedure analogous to **A** for **1a**. An identical workup gave **1c** as a colorless oil (3.12 g, 9.43 mmol, 90%). **B.**[24] $PhPH_2$ (1.028 g, 9.337 mmol), THF (40 mL), *n*-BuLi (2.5 M in hexanes, 7.50 mL, 18.70 mmol), and $Br(CH_2)_6CH{=}CH_2$ (3.59 g, 3.15 mL, 18.7 mmol) were combined in a procedure analogous to **B** for **1a**. An identical workup gave **1c** as a bright yellow oil (1.82 g, 5.51 mmol, 59%). NMR ($CDCl_3$, δ in ppm): ^1H (400 MHz) 7.50 (dt, J_{HH} = 1.8 Hz, J_{HH} = 7.5 Hz, 2H, Ph), 7.37−7.29 (m, 3H, Ph), 5.78 (tdd, $^3J_{HH}$ = 6.7 Hz, $^3J_{HHcis}$ = 10.2 Hz, $^3J_{HHtrans}$ = 16.9 Hz, 2H, C*H*=), 5.03−4.89 (m, 4H, =CH_2), 1.98−1.90 (m, 4H, CH_2), 1.75−1.60 (m, 4H, CH_2), 1.55−1.22 (m, 16H, CH_2); $^{13}C\{^1H\}$ (100 MHz)[15] 139.1 (d, $^1J_{CP}$ = 14.6 Hz, *i*-Ph), 139.0 (s, CH=), 132.2 (d, $^2J_{CP}$ = 18.5 Hz, *o*-Ph), 128.5 (s, *p*-Ph), 128.2 (d, $^3J_{CP}$ = 6.8 Hz, *m*-Ph), 114.1 (s, =CH_2), 33.7 (s, CH_2), 31.1 (d, J_{CP} = 11.4 Hz, CH_2), 28.4 (s, 2CH_2), 28.3 (d, $^3J_{CP}$ = 12.8 Hz, CH_2), 25.9 (d, $^1J_{CP}$ = 13.6 Hz, PCH_2);[25] $^{31}P\{^1H\}$ (162 MHz) −23.3 (s).

***trans*-$Fe(CO)_3(PhP((CH_2)_4CH{=}CH_2)_2)_2$ (2a).** A Schlenk flask was charged with $Fe(CO)_3(\eta^4$-benzylideneacetone) (0.6234 g, 2.179 mmol),[13] THF (40 mL), and **1a** (1.375 g, 5.012 mmol). The red-brown mixture was stirred for 15 h and turned yellow. The solvent was removed by oil pump vacuum. The residue was extracted with hexanes. The extracts were filtered through neutral alumina (7 × 3.5 cm), which was washed with hexanes and then hexanes/CH_2Cl_2 (67:33 v/v). The solvent was removed from the combined filtrates by oil pump vacuum to give **2a**·$(C_6H_{14})_{0.5}$ as a yellow-brownish oil (0.4482 g, 0.6125 mmol, 28%). Anal. Calcd for $C_{39}H_{54}FeO_3P_2\cdot(C_6H_{14})_{0.5}$ (731.74): C 68.95, H, 8.40. Found: C 69.19, H, 8.49. NMR (C_6D_6, δ in ppm): ^1H (400 MHz) 8.05−8.03 (m, 4H, Ph), 7.34−7.13 (m, 6H, Ph), 5.79 (tdd, $^3J_{HH}$ = 6.6 Hz, $^3J_{HHcis}$ = 10.0 Hz, $^3J_{HHtrans}$ = 13.4 Hz, 4H, C*H*=), 5.15−4.98 (m, 8H, =CH_2), 2.33−2.06 (m, 8H, CH_2), 2.06−1.96 (m, 8H, CH_2) 1.88−1.50 (m, 12H, CH_2), 1.46−1.18 (m, 4H, CH_2, 4H, C_6H_{14} solvate), 1.15−0.82 (m, 3H, C_6H_{14}); $^{13}C\{^1H\}$ (100 MHz)[15,26,27] 215.3 (t, $^2J_{CP}$ = 28.7 Hz, CO), 138.5 (s, CH=), 131.8 (virtual t,[14] $^2J_{CP}$ = 4.4 Hz, *o*-Ph), 130.0 (s, *p*-Ph), 128.7 (virtual t,[14] $^3J_{CP}$ = 4.2 Hz, *m*-Ph), 114.9 (s, =CH_2), 33.5 (s, CH_2), 33.1−32.8 (m, PCH_2), 30.5 (virtual t,[14] $^3J_{CP}$ = 6.6 Hz, $PCH_2CH_2CH_2$), 24.0 (s, PCH_2CH_2); $^{31}P\{^1H\}$ (162 MHz) 70.2 (s). IR (cm^{-1}, oil film): 2940 (m), 2875 (w), 1861 (s, ν_{CO}), 1873 (m), 1475 (m), 953 (m). MS:[28] 630 ([M − 3CO]$^+$, 1%).

***trans*-$Fe(CO)_3(PhP((CH_2)_5CH{=}CH_2)_2)_2$ (2b).** $Fe(CO)_3(\eta^4$-benzylideneacetone) (0.8024 g, 2.805 mmol),[13] THF (40 mL), and **1b** (1.6964 g, 5.609 mmol) were combined in a procedure analogous to that for **2a**. An identical workup gave **2b**·$(C_6H_{14})_{0.5}$ as a yellow-brownish oil (1.539 g, 1.953 mmol, 70%). Anal. Calcd for $C_{43}H_{62}FeO_3P_2\cdot(C_6H_{14})_{0.5}$ (787.85): C 70.13, H 8.83. Found: C 70.03, H 7.96.[29] NMR (C_6D_6, δ in ppm): ^1H (400 MHz) 8.03−7.99 (m, 4H, Ph), 7.34−7.20 (m, 6H, Ph), 5.82 (tdd, $^3J_{HH}$ = 6.7 Hz, $^3J_{HHcis}$ = 10.1 Hz, $^3J_{HHtrans}$ = 16.9 Hz, 4H, C*H*=), 5.12−5.04 (m, 8H, =CH_2), 2.32−2.10 (m, 8H, CH_2), 2.10−1.92 (m, 8H, CH_2), 1.90−1.64 (m, 8H, CH_2), 1.48−1.27 (m, 16H, CH_2, 4H, C_6H_{14}), 0.98−0.86 (m, 3H, C_6H_{14}); $^{13}C\{^1H\}$ (100 MHz)[15,27] 215.6 (t, $^2J_{CP}$ = 28.6 Hz, CO), 138.9 (s, CH=), 136.4 (apparent dd, $^1J_{CP}$, $^3J_{CP}$ = 21.5, 17.4 Hz, *i*-Ph), 131.9 (virtual t,[14] $^2J_{CP}$ = 4.7 Hz, *o*-Ph), 130.2 (s, *p*-Ph), 128.7 (virtual t,[14] $^3J_{CP}$ = 4.4 Hz, *m*-Ph), 114.7 (s, =CH_2), 33.8 (s, CH_2), 33.1 (apparent dd, $^1J_{CP}$, $^3J_{CP}$ = 15.4, 13.5 Hz, PCH_2), 30.8 (virtual t,[14] $^3J_{CP}$ = 6.6 Hz, $PCH_2CH_2CH_2$), 28.7 (s, CH_2), 24.4 (s, PCH_2CH_2); $^{31}P\{^1H\}$ (162 MHz) 69.0 (s). IR (cm^{-1}, oil film): 2943 (m), 2878 (w), 1864 (s, ν_{CO}), 1477 (m), 957 (m). MS:[28] 743 ([M]$^+$, 8%), 689 ([M − 2CO]$^+$, 1%), 660 ([M − 3CO]$^+$, 358 ([Fe + **1b**]$^+$, 100%), 303 ([**1b**]$^+$, 17%).

***trans*-$Fe(CO)_3(PhP((CH_2)_6CH{=}CH_2)_2)_2$ (2c).** $Fe(CO)_3(\eta^4$-benzylideneacetone) (0.6297 g, 2.201 mmol),[13] THF (40 mL), and **1c** (1.455 g, 4.402 mmol) were combined in a procedure analogous to that for **2a**. An identical workup gave **2c**·$(C_6H_{14})_2$ as a yellow-brownish oil (0.7892 g, 0.8109 mmol, 37%). Anal. Calcd for $C_{47}H_{70}FeO_3P_2\cdot(C_6H_{14})_2$ (973.22): C 72.81, H 10.15. Found: C 73.15, H 9.46.[29] NMR (C_6D_6, δ in ppm): ^1H (400 MHz) 8.01−7.92 (m, 4H, Ph), 7.26−7.02 (m, 6H, Ph), 5.75 (tdd, $^3J_{HH}$ = 6.7 Hz, $^3J_{HHcis}$ = 10.1 Hz, $^3J_{HHtrans}$ = 16.9 Hz, 4H, C*H*=), 5.09−4.92 (m, 8H, =CH_2), 2.29−2.08 (m, 8H, CH_2), 2.02−1.88 (m, 8H, CH_2), 1.86−1.62 (m, 8H, CH_2), 1.38−1.15 (m, 24H, CH_2, 22 H, C_6H_{14}), 0.98−0.86 (m, 6H, C_6H_{14}); $^{13}C\{^1H\}$ (100 MHz)[15,27] 215.7 (t, $^2J_{CP}$ = 28.5 Hz, CO) 139.1 (s, CH=), 136.5 (apparent dd, $^1J_{CP}$, $^3J_{CP}$ = 17.6, 21.4 Hz, *i*-Ph), 131.8 (virtual t,[14] $^2J_{CP}$ = 4.6 Hz, *o*-Ph), 129.9 (s, *p*-Ph), 128.7 (virtual t,[14] $^3J_{CP}$ = 4.5 Hz, *m*-Ph), 114.5 (s, =CH_2), 34.1 (s, CH_2), 33.2 (apparent dd, $^1J_{CP}$, $^3J_{CP}$ = 15.9, 12.5 Hz, PCH_2), 31.4 (virtual t,[14] $^3J_{CP}$ = 6.6 Hz, $PCH_2CH_2CH_2$), 29.1 (s, CH_2), 29.0 (s, CH_2), 24.6 (s, PCH_2CH_2); $^{31}P\{^1H\}$ (162 MHz) 69.8 (s). IR (cm^{-1}, oil film): 2927 (s), 2858 (m), 1869 (m, ν_{CO}), 1437 (m), 1174 (s), 911 (s). MS:[28] 800 ([M]$^+$, 3%), 716 ([M − 3CO]$^+$, 24%), 368 ([Fe + **1c**]$^+$, 100%), 331 ([**1c**]$^+$, 16%).

***trans*-$Fe(CO)_3(PhP((CH_2)_4CH{=}CH(CH_2)_4)_2PPh)$ (3a).** A Schlenk flask was charged with **2a** (0.2241 g, 0.3254 mmol) and CH_2Cl_2 (325 mL; the resulting solution was 0.00099 M in **2a**) and heated to 45 °C. Then, Grubbs' first generation catalyst (0.0201 g, 0.0244 mmol) was added with stirring. After 2 h, another charge of Grubbs' catalyst (0.0201 g, 0.0244 mmol) was added. After 15 h, the mixture was cooled and the solvent was removed by oil pump vacuum. The residue was extracted with hexanes. The extracts were filtered through neutral alumina (7 × 2.5 cm), which was rinsed with additional hexanes. The solvent was removed from the filtrate by oil pump vacuum to give a mixture of **3a** and oligomers as a yellow solid (0.0625 g, 0.0988 mmol, 30%). NMR (C_6D_6, δ in ppm): ^1H (400 MHz) 8.06−8.01 (m, 4H, Ph), 7.52−7.03 (m, 6H, Ph), 5.59−5.30 (m, 4H, C*H*=), 2.53−0.82 (m, 32H, CH_2); $^{13}C\{^1H\}$ (100 MHz)[30] 214.44 (t, $^2J_{CP}$ = 26.4 Hz, 2CO), 214.38 (t, $^2J_{CP}$ = 33.2 Hz, CO), 132.0 (s, CH=), 131.7 (virtual t,[14] $^2J_{CP}$ = 5.1 Hz, *o*-Ph), 130.8 (obscured dd, one of two central peaks, *i*-Ph), 130.8 (s, *p*-Ph), 128.8 (virtual t,[14] $^3J_{CP}$ = 4.6 Hz, *m*-Ph), 33.1 (s, CH_2), 33.5 (apparent dd, $^1J_{CP}$, $^3J_{CP}$ = 15.5, 13.3 Hz, PCH_2), 30.9 (virtual t,[14] $^3J_{CP}$ = 7.7 Hz, $PCH_2CH_2CH_2$), 24.6 (s, PCH_2CH_2); $^{31}P\{^1H\}$ (162 MHz) 79.3 (s, 53%), 75.9 (s, 6%), 73.8−72.6 (overlapping signals, 41%). MS:[28] 632 ([M]$^+$, 25%), 606 ([M − CO]$^+$, 13%), 576 ([M − 2CO]$^+$, 20%), 548 ([M − 3CO]$^+$, 100%).

DOI: 10.1021/acs.organomet.7b00330
Organometallics XXXX, XXX, XXX−XXX

***trans*-Fe(CO)$_3$(PhP((CH$_2$)$_5$CH═CH(CH$_2$)$_5$)$_2$PPh) (3b).** Complex **2b** (0.5213 g, 0.6999 mmol), CH_2Cl_2 (700 mL; the resulting solution was 0.00089 M in **2b**), and Grubbs' first generation catalyst (0.0431 g, 0.0525 mmol and then 0.0432 g, 0.0525 mmol) were combined in a procedure analogous to that for **3a**. A similar workup (neutral alumina 10 × 2.5 cm) gave a mixture of **3b** and oligomers as a yellow solid (0.1494 g, 0.2170 mmol, 31%). NMR (C_6D_6, δ in ppm): ^{1}H (400 MHz) 8.19−8.01 (m, 4H, Ph), 7.37−7.18 (m, 6H, Ph), 5.99−5.48 (m, 4H, C*H*═), 2.55−1.12 (m, 40H, C*H*$_2$); ^{31}P{^{1}H} (162 MHz) 73.5 (s, 35%), 73.1 (s, 31%), 72.7 (s, 8%), 71.5 (s, 15%), 71.3 (s, 11%).

***trans*-Fe(CO)$_3$(PhP((CH$_2$)$_6$CH═CH(CH$_2$)$_6$)$_2$PPh) (3c).** Complex **2c** (0.4025 g, 0.5025 mmol), CH_2Cl_2 (503 mL; the resulting solution was 0.00099 M in **2c**), and Grubbs' first generation catalyst (0.0310 g, 0.0377 mmol and then 0.0310 g, 0.0377 mmol) were combined in a procedure analogous to that for **3a**. The residue was extracted with hexanes/CH_2Cl_2 (84:16 v/v). The extracts were filtered through neutral alumina (12 × 2.5 cm), which was rinsed with additional hexanes/CH_2Cl_2. The solvent was removed from the filtrate by oil pump vacuum to give a mixture of **3c** and oligomers (0.1160 g, 0.1558 mmol, 31%). NMR (C_6D_6, δ in ppm): ^{1}H (400 MHz) 8.21−8.06 (m, 4H, Ph), 7.46−7.11 (m, 6H, Ph), 5.62−5.21 (m, 4H, C*H*═), 2.49−0.98 (m, 48H, C*H*$_2$); ^{31}P{^{1}H} (162 MHz) 73.9 (s, 63%), 73.3 (s, 13%), 73.1 (s, 14%), 72.5 (s, 4%), 72.3 (s, 6%).

***trans*-Fe(CO)$_3$(PhP((CH$_2$)$_{10}$)$_2$PPh) (4a).** A Fisher−Porter bottle was charged with **3a** (0.2164 g, 0.3421 mmol), Rh(Cl)(PPh$_3$)$_3$ (0.0633 g, 0.0648 mmol), THF (20 mL), and H_2 (5 bar). The mixture was stirred. After 15 h, the solvent was removed by oil pump vacuum. The residue was extracted with hexanes/CH_2Cl_2 (92:8 v/v). The extract was filtered through neutral alumina (12 × 2.5 cm), which was rinsed with hexanes/CH_2Cl_2 (92:8 v/v). The solvent was removed from the filtrate by oil pump vacuum to give **4a** as a white-yellow gum (0.1502 g, 0.2360 mmol, 69%). NMR (C_6D_6, δ in ppm): ^{1}H (400 MHz) 8.11−7.89 (m, 4H, Ph), 7.31−6.95 (m, 6H, Ph), 2.22−1.68 (m, 12H, C*H*$_2$), 1.58−1.38 (m, 20H, C*H*$_2$), 1.37−0.85 (m, 8H, C*H*$_2$); ^{13}C{^{1}H} (100 MHz)[15] 216.5 (t, $^2J_{CP}$ = 28.5 Hz, CO), 215.1 (t, $^2J_{CP}$ = 26.8 Hz, 2CO), 136.5 (apparent dd, $^1J_{CP}$, $^3J_{CP}$ = 20.3, 17.3 Hz, *i*-Ph), 132.1 (virtual t,[14] $^2J_{CP}$ = 5.1 Hz, *o*-Ph), 130.1 (br s, *p*-Ph), 128.8 (virtual t,[14] $^3J_{CP}$ = 4.5 Hz, *m*-Ph), 32.4 (apparent dd, $^1J_{CP}$, $^3J_{CP}$ = 15.5, 13.6 Hz, PCH$_2$),[31] 29.0 (virtual t,[14] $^3J_{CP}$ = 6.2 Hz, PCH$_2$CH$_2$CH$_2$),[31] 27.6 (s, CH$_2$), 25.4 (s, CH$_2$), 24.1 (s, PCH$_2$CH$_2$);[31] ^{31}P{^{1}H} (162 MHz) 78.0 (s). MS:[28] 636 ([M]$^+$, 5%), 552 ([M − 3CO]$^+$, 100%).

***trans*-Fe(CO)$_3$(PhP((CH$_2$)$_{12}$)$_2$PPh) (4b).** A Fisher−Porter bottle was charged with **3b** (0.3051 g, 0.2443 mmol), PtO_2 (0.0194 g, 0.0855 mmol), THF (20 mL), and H_2 (5 bar). The mixture was stirred. After 15 h, the solvent was removed by oil pump vacuum. The residue was extracted with hexanes/CH_2Cl_2 (75:25 v/v). The extract was filtered through neutral alumina (12 × 2.5 cm), which was rinsed with hexanes/CH_2Cl_2. The solvent was removed from the filtrate by oil pump vacuum to give **4b** as a white wax (0.133 g, 0.1881 mmol, 77%). Anal. Calcd for $C_{39}H_{58}FeO_3P_2$ (692.68): C 67.63, H 8.44. Found: C 67.60, H, 10.20.[29] NMR (C_6D_6, δ in ppm): ^{1}H (400 MHz) 8.12−7.98 (m, 4H, Ph), 7.36−7.11 (m, 6H, Ph), 2.18−1.14 (m, 48H, C*H*$_2$); ^{13}C{^{1}H} (100 MHz)[15] 215.4 (t, $^2J_{CP}$ = 29.1 Hz, CO), 136.8 (apparent dd, $^1J_{CP}$, $^3J_{CP}$ = 21.0, 17.1 Hz, *i*-Ph), 132.1 (virtual t,[14] $^2J_{CP}$ = 5.0 Hz, *o*-Ph), 130.0 (br s, *p*-Ph), 128.8 (virtual t,[14] $^3J_{CP}$ = 4.6 Hz, *m*-Ph), 34.0 (apparent dd, $^1J_{CP}$, $^3J_{CP}$ = 15.7, 13.7 Hz, PCH$_2$),[31] 29.7 (virtual t,[14] $^3J_{CP}$ = 7.3 Hz, PCH$_2$CH$_2$CH$_2$),[31] 27.7 (s, CH$_2$), 27.4 (s, CH$_2$), 26.4 (s, CH$_2$), 23.2 (s, PCH$_2$CH$_2$);[31] ^{31}P{^{1}H} (162 MHz) 72.6 (s). IR (cm^{-1}, oil film): 2927 (m), 2858 (m), 1861 (s, ν_{CO}), 1460 (w), 1097 (m), 1020 (m). MS:[28] 692 ([M]$^+$, 6%), 636 ([M − 2CO]$^+$, 7%), 608 ([M − 3CO]$^+$, 100%).

***trans*-Fe(CO)$_3$(PhP((CH$_2$)$_{14}$)$_2$PPh) (4c).** Complex **3c** (0.4025 g, 0.5404 mmol), Rh(Cl)(PPh$_3$)$_3$ (0.0749 g, 0.0811 mmol), THF (20 mL), and H_2 (5 bar) were combined in a procedure analogous to that for **4a**. An identical workup gave **4c** as a white-yellow gum (0.2953 g, 0.3945 mmol, 73%). NMR (C_6D_6, δ in ppm): ^{1}H (400 MHz) 8.21−8.08 (m, 4H, Ph), 7.47−7.18 (m, 6H, Ph), 2.21−2.10 (m, 8H, C*H*$_2$), 2.10−1.82 (m, 8H, C*H*$_2$), 1.82−1.21 (m, 40H, C*H*$_2$); ^{13}C{^{1}H} (100 MHz)[15] 214.1 (t, $^2J_{CP}$ = 28.8 Hz, CO), 136.9 (apparent dd, $^1J_{CP}$, $^3J_{CP}$ = 21.0, 16.9 Hz, *i*-Ph), 132.2 (virtual t,[14] $^2J_{CP}$ = 4.6 Hz, *o*-Ph), 130.2 (s, *p*-Ph), 128.9 (virtual t,[14] $^3J_{CP}$ = 4.2 Hz, *m*-Ph), 34.0 (virtual t,[14] $^1J_{CP}$ = 13.6 Hz, PCH$_2$),[31] 31.1 (virtual t,[14] $^3J_{CP}$ = 6.9 Hz, PCH$_2$CH$_2$CH$_2$),[31] 28.3 (s, CH$_2$), 28.1 (s, CH$_2$), 27.4 (s, CH$_2$), 26.7 (s, CH$_2$), 24.7 (s, PCH$_2$CH$_2$);[31] ^{31}P{^{1}H} (162 MHz) 72.0 (s). IR (cm^{-1}, oil film): 2927 (s), 2858 (m), 1869 (s, ν_{CO}), 1259 (s), 1089 (s), 1020 (s). MS:[28] 748 ([M]$^+$, 7%), 692 ([M − 2CO]$^+$, 4%), 664 ([M − 3CO]$^+$, 100%).

Crystallography. A. Crude **3a** was suspended in methanol and warmed. THF was added until the sample was homogeneous. After 1 day, colorless prisms of (*E*,*E*)-**3a** had formed. Data were collected using a Nonius Kappa CCD area detector as outlined in Table S1. Cell parameters were obtained from 10 frames using a 10° scan and refined with 3445 reflections. Lorentz, polarization, and absorption corrections[32] were applied. The space group was determined from systematic absences and subsequent least-squares refinement. The structure was solved by direct methods. The parameters were refined with all data by full-matrix least-squares on F^2 using SHELXL-97 (racemic twin, 56:44).[33] Non-hydrogen atoms were refined with anisotropic thermal parameters. The hydrogen atoms were fixed in idealized positions using a riding model. Scattering factors were taken from the literature.[34] **B.** Complex **4b** was dissolved in hexanes. After 4 days, colorless needles had formed. Data were collected as with **3a**. Cell parameters were obtained from 10 frames using a 10° scan and refined with 8473 reflections, and the structure was solved identically to **3a**.

Calculations. Computations were performed using the Gaussian09 program package, employing the ultrafine grid (99 590) to enhance accuracy.[35] Geometries were optimized using density functional theory and the B3LYP,[36] TPSS,[37] and CAM-B3LYP[38] functionals with an all-electron 6-311+G(d,p)[39] basis set on all atoms except iron, which was treated with a pseudopotential.[40] Frequency calculations were performed at the same level to characterize the optimized geometries.

■ ASSOCIATED CONTENT

Supporting Information

The Supporting Information is available free of charge on the ACS Publications website at DOI: 10.1021/acs.organomet.7b00330.

Table of crystallographic data, additional preparative and spectroscopic data, calculations of $\Delta G^{\ddagger}$ values, and data from DFT computations (PDF)

Molecular structure file that can be read by the program Mercury[41] and contains the optimized geometries of all computed structures[42] (MOL)

Accession Codes

CCDC 1546130−1546131 contain the supplementary crystallographic data for this paper. These data can be obtained free of charge via www.ccdc.cam.ac.uk/data_request/cif, or by emailing data_request@ccdc.cam.ac.uk, or by contacting The Cambridge Crystallographic Data Centre, 12 Union Road, Cambridge CB2 1EZ, UK; fax: +44 1223 336033.

■ AUTHOR INFORMATION

Corresponding Author

*E-mail: gladysz@mail.chem.tamu.edu.

ORCID

John A. Gladysz: 0000-0002-7012-4872

Notes

The authors declare no competing financial interest.

■ ACKNOWLEDGMENTS

The authors thank the U.S. National Science Foundation (CHE-1153085, CHE-156601) and Deutsche Forschungsgemeinschaft (DFG, GL 300/9-1) for support, the Laboratory for Molecular Simulation and Texas A&M High Performance Research

Computing for resources, Prof. Michael B. Hall for helpful discussions, and Dr. Tobias Fiedler for assistance in preparing the manuscript.

REFERENCES

(1) Fiedler, T.; Gladysz, J. A. Review: Multifold Ring Closing Olefin Metatheses in Syntheses of Organometallic Molecules with Unusual Connectivities. In *Olefin Metathesis: Theory and Practice*; Grela, K., Ed.; John Wiley & Sons: Hoboken, NJ, 2014; pp 311−328.

(2) Representative examples since the coverage in ref 1: (a) Danon, J. J.; Krüger, A.; Leigh, D. A.; Lemonnier, J.-F.; Stephens, A. J.; Vitorica-Yrezabal, I. J.; Woltering, S. L. *Science* **2017**, *355*, 159−162. (b) Ogasawara, M.; Tseng, Y.-Y.; Liu, Q.; Chang, N.; Yang, X.; Takahashi, T.; Kamikawa, K. *Organometallics* **2017**, *36*, 1430−1435 and earlier papers by this group cited therein. (c) Masuda, T.; Arase, J.; Inagaki, Y.; Kawahata, M.; Yamaguchi, K.; Ohhara, T.; Nakao, A.; Momma, H.; Kwon, E.; Setaka, W. *Cryst. Growth Des.* **2016**, *16*, 4392−4401 and earlier papers by this group cited therein. (d) Gil-Ramírez, G.; Hoekman, S.; Kitching, M. O.; Leigh, D. A.; Vitorica-Yrezabal, I. J.; Zhang, G. *J. Am. Chem. Soc.* **2016**, *138*, 13159−13162. (e) Cain, M. F.; Forrest, W. P., Jr.; Peryshkov, D. V.; Schrock, R. R.; Müller, P. *J. Am. Chem. Soc.* **2013**, *135*, 15338−15341.

(3) (a) Ruwwe, J.; Martín-Alvarez, J. M.; Horn, C. R.; Bauer, E. B.; Szafert, S.; Lis, T.; Hampel, F.; Cagle, P. C.; Gladysz, J. A. *Chem. - Eur. J.* **2001**, *7*, 3931−3950. (b) Bauer, E. B.; Hampel, F.; Gladysz, J. A. *Organometallics* **2003**, *22*, 5567−5580. (c) Shima, T.; Bauer, E. B.; Hampel, F.; Gladysz, J. A. *Dalton Trans.* **2004**, 1012−1018.

(4) Analogous alkyne metatheses: (a) Bauer, E. B.; Szafert, S.; Hampel, F.; Gladysz, J. A. *Organometallics* **2003**, *22*, 2184−2186. (b) Bauer, E. B.; Hampel, F.; Gladysz, J. A. *Adv. Synth. Catal.* **2004**, *346*, 812−822.

(5) (a) Shima, T.; Hampel, F.; Gladysz, J. A. *Angew. Chem., Int. Ed.* **2004**, *43*, 5537−5540; *Angew. Chem.* **2004**, *116*, 5653−5656. (b) Lang, G. M.; Shima, T.; Wang, L.; Cluff, K. J.; Skopek, K.; Hampel, F.; Blumel, J.; Gladysz, J. A. *J. Am. Chem. Soc.* **2016**, *138*, 7649−7663. (c) Lang, G. M.; Skaper, D.; Hampel, F.; Gladysz, J. A. *Dalton Trans.* **2016**, *45*, 16190−16204.

(6) (a) Nawara, A. J.; Shima, T.; Hampel, F.; Gladysz, J. A. *J. Am. Chem. Soc.* **2006**, *128*, 4962−4963. (b) Nawara-Hultzsch, A. J.; Stollenz, M.; Barbasiewicz, M.; Szafert, S.; Lis, T.; Hampel, F.; Bhuvanesh, N.; Gladysz, J. A. *Chem. - Eur. J.* **2014**, *20*, 4617−4637. (c) Taher, D.; Nawara-Hultzsch, A. J.; Bhuvanesh, N.; Hampel, F.; Gladysz, J. A. *J. Organomet. Chem.* **2016**, *821*, 136−141. (e) Kharel, S.; Joshi, H.; Bierschenk, S.; Stollenz, M.; Taher, D.; Bhuvanesh, N.; Gladysz, J. A. *J. Am. Chem. Soc.* **2017**, *139*, 2172−2175.

(7) Wang, L.; Hampel, F.; Gladysz, J. A. *Angew. Chem., Int. Ed.* **2006**, *45*, 4372−4375; *Angew. Chem.* **2006**, *118*, 4479−4482.

(8) (a) Wang, L.; Shima, T.; Hampel, F.; Gladysz, J. A. *Chem. Commun.* **2006**, 4075−4077. (b) Estrada, A. L.; Jia, T.; Bhuvanesh, N.; Blümel, J.; Gladysz, J. A. *Eur. J. Inorg. Chem.* **2015**, *2015*, 5318−5321.

(9) (a) Hess, G. D.; Hampel, F.; Gladysz, J. A. *Organometallics* **2007**, *26*, 5129−5131. (b) Hess, G. D.; Fiedler, T.; Hampel, F.; Gladysz, J. A. *Inorg. Chem.* **2017**, DOI: 10.1021/acs.inorgchem.7b00909.

(10) (a) Fiedler, T.; Bhuvanesh, N.; Hampel, F.; Reibenspies, J. H.; Gladysz, J. A. *Dalton Trans.* **2016**, *45*, 7131−7147. (b) Fiedler, T.; Chen, L.; Wagner, N. D.; Russell, D. R.; Gladysz, J. A. *Organometallics* **2016**, *35*, 2071−2075.

(11) Skopek, K.; Gladysz, J. A. *J. Organomet. Chem.* **2008**, *693*, 857−866.

(12) Lang, G. M.; Bhuvanesh, N.; Reibenspies, J. H.; Gladysz, J. A. *Organometallics* **2016**, *35*, 2873−2889.

(13) (a) Howell, J. A. S.; Josty, P. L.; Johnson, B. F. G.; Lewis, J. *J. Organomet. Chem.* **1972**, *39*, 329−333. (b) Brookhart, M.; Nelson, G. O. *J. Organomet. Chem.* **1979**, *164*, 193−202.

(14) Hersh, W. H. *J. Chem. Educ.* **1997**, *74*, 1485−1488. The *J* values reported for virtual triplets represent the apparent couplings between adjacent peaks and not the mathematically rigorous coupling constants.

(15) The PC_6H_5 $^{13}C\{^1H\}$ NMR signals were assigned as described by Mann, B. E. *J. Chem. Soc., Perkin Trans. 2* **1972**, 30−34. That with the chemical shift closest to benzene was attributed to the *meta* carbon, and the least intense to the *ipso* carbon. See also Jolly, P. W.; Mynott, R. *Adv. Organomet. Chem.* **1981**, *19*, 257−304.

(16) Among three diarsine analogues **IIIb**, there is one exception.[12]

(17) (a) Bondi, A. *J. Phys. Chem.* **1964**, *68*, 441−451. (b) Mantina, M.; Chamberlin, A. C.; Valero, R.; Cramer, C. J.; Truhlar, D. G. *J. Phys. Chem. A* **2009**, *113*, 5806−5812.

(18) Sandström, J. *Dynamic NMR Spectroscopy*; Academic Press: New York, 1982; pp 93−123.

(19) Specifically, *trans*-$Pt(Cl)_2(P((CH_2)_6CH{=}CH_2)_3)_2$ undergoes metathesis/hydrogenation to give a product of the type **IIIa** in ca. 40% yield, but when one of the chloride ligands is replaced by pentafluorophenyl, only oligomers or polymers are obtained.[6b]

(20) Lang, G. M.; Skaper, D.; Shima, T.; Otto, M.; Wang, L.; Gladysz, J. A. *Aust. J. Chem.* **2015**, *68*, 1342−1351.

(21) Ansyln, E. V.; Dougherty, D. A. *Modern Physical Organic Chemistry*; University Science Books: Sausalito, CA, 2006; pp 97−98.

(22) It may be possible to extract more quantitative data from the low-temperature $^{13}C\{^1H\}$ spectra by using **4b** that has been slightly enriched in ^{13}CO.

(23) To help understand the basis for the energy order **4′a−c** > **4a−c**, the $Fe(CO)_3$ moieties were excised while leaving the geometries of the ligand scaffolds intact. Single-point calculations were then carried out. The energy differences between the ligand scaffolds were essentially unchanged relative to those of **4′a−c** and **4a−c**. Thus, these stability differences are almost entirely due to differences in ring strain. When the same protocol was applied to **4″a−c** and **4a−c**, the energy differences became lower (but still pronounced). This indicates that the energy order **4″a−c** > **4a−c** is in part due to greater steric interactions of the carbonyl groups with the methylene chains and phenyl groups in the former.

(24) Smaller-scale versions of the phosphine syntheses that utilize $PhPH_2$ have been reported (with microanalyses) in refs 3a and c.

(25) The PCH_2 signal assignment was made by analogy to that confirmed for the related phosphines $P((CH_2)_mCH{=}CH_2)_3$: Nawara-Hultzsch, A. J.; Skopek, K.; Shima, T.; Barbasiewicz, M.; Hess, G. D.; Skaper, D.; Gladysz, J. A. *Z. Naturforsch., B: J. Chem. Sci.* **2010**, *65b*, 414−424.

(26) The *i*-Ph signal (virtual t) was not observed.

(27) The $PCH_2CH_2CH_2$ ^{13}C NMR signals were assigned by analogy to those rigorously established for the closely related acyclic complexes *trans*-$Fe(CO)_3(P((CH_2)_mCH{=}CH_2)_3)_2$ in ref 20.

(28) FAB (3-nitrobenzyl alcohol matrix); *m/z* (relative intensity, %); the most intense peak of the isotope envelope is given.

(29) This hydrogen analysis poorly agrees with the empirical formula but is nonetheless reported as the best obtained to date. Note that solvates are verified by ^1H NMR.

(30) These $^{13}C\{^1H\}$ NMR data are taken from a second preparation given in the Supporting Information (higher concentration and catalyst loading). The workup gave a lower yield (20%) of a product that was homogeneous by $^{31}P\{^1H\}$ NMR and showed fewer byproduct peaks in other NMR spectra.

(31) The $PCH_2CH_2CH_2$ $^{13}C\{^1H\}$ NMR signals were assigned by analogy to those rigorously established for the closely related gyroscope-like complexes *trans*-$Fe(CO)_3(P((CH_2)_n)_3P)$ in ref 5b.

(32) (a) Hooft, R. W. W. *Collect*; data collection software; Nonius BV: Delft, The Netherlands, 1998. (b) Otwinowski, Z.; Minor, W. In *Methods in Enzymology*; Carter, C. W., Jr., Sweet, R. M., Eds.; Macromolecular Crystallography, Vol. *276*, Part A; Academic Press: New York, 1997; pp 307−326.

(33) Sheldrick, G. M. *Acta Crystallogr.* **2015**, *C71*, 3−8.

(34) Cromer, D. T.; Waber, J. T. In *International Tables for X-ray Crystallography*; Ibers, J. A., Hamilton, W. C., Eds.; Kynoch: Birmingham, England, 1974.

(35) Frisch, M. J.; Trucks, G. W.; Schlegel, H. B.; Scuseria, G. E.; Robb, M. A.; Cheeseman, J. R.; Scalmani, G.; Barone, V.; Mennucci, B.; Petersson, G. A.; Nakatsuji, H.; Caricato, M.; Li, X.; Hratchian, H. P.; Izmaylov, A. F.; Bloino, J.; Zheng, G.; Sonnenberg, J. L.; Hada, M.; Ehara, M.; Toyota, K.; Fukuda, R.; Hasegawa, J.; Ishida, M.; Nakajima,

DOI: 10.1021/acs.organomet.7b00330
Organometallics XXXX, XXX, XXX−XXX

T.; Honda, Y.; Kitao, O.; Nakai, H.; Vreven, T.; Montgomery, J. A., Jr.; Peralta, J. E.; Ogliaro, F.; Bearpark, M.; Heyd, J. J.; Brothers, E.; Kudin, K. N.; Staroverov, V. N.; Kobayashi, R.; Normand, J.; Raghavachari, K.; Rendell, A.; Burant, J. C.; Iyengar, S. S.; Tomasi, J.; Cossi, M.; Rega, N.; Millam, J. M.; Klene, M.; Knox, J. E.; Cross, J. B.; Bakken, V.; Adamo, C.; Jaramillo, J.; Gomperts, R.; Stratmann, R. E.; Yazyev, O.; Austin, A. J.; Cammi, R.; Pomelli, C.; Ochterski, J. W.; Martin, R. L.; Morokuma, K.; Zakrzewski, V. G.; Voth, G. A.; Salvador, P.; Dannenberg, J. J.; Dapprich, S.; Daniels, A. D.; Farkas, Ö.; Foresman, J. B.; Ortiz, J. V.; Cioslowski, J.; Fox, D. J. *Gaussian 09*, revision D.01; Gaussian, Inc.: Wallingford, CT, 2009.

(36) (a) Becke, A. D. *Phys. Rev. A: At., Mol., Opt. Phys.* **1988**, *38*, 3098−3100. (b) Becke, A. D. *J. Chem. Phys.* **1993**, *98*, 5648−5652. (c) Lee, C.; Yang, W.; Parr, R. G. *Phys. Rev. B: Condens. Matter Mater. Phys.* **1988**, *37*, 785−789.

(37) Tao, J. M.; Perdew, J. P.; Staroverov, V. N.; Scuseria, G. E. *Phys. Rev. Lett.* **2003**, *91*, 146401−146404.

(38) Yanai, T.; Tew, D. P.; Handy, N. C. *Chem. Phys. Lett.* **2004**, *393*, 51−57.

(39) Hariharan, P. C.; Pople, J. A. *Theor. Chim. Acta* **1973**, *28*, 213−222.

(40) (a) Dolg, M.; Wedig, U.; Stoll, H.; Preuss, H. *J. Chem. Phys.* **1987**, *86*, 866−872. (b) Martin, J. M. L.; Sundermann, A. *J. Chem. Phys.* **2001**, *114*, 3408−3420.

(41) Macrae, C. F.; Bruno, I. J.; Chisholm, J. A.; Edgington, P. R.; McCabe, P.; Pidcock, E.; Rodriguez-Monge, L.; Taylor, R.; van de Streek, J.; Wood, P. A. *J. Appl. Crystallogr.* **2008**, *41*, 466−470.

(42) Lichtenberger, D. L.; Gladysz, J. A. *Organometallics* **2014**, *33*, 835.

DOI: 10.1021/acs.organomet.7b00330
Organometallics XXXX, XXX, XXX−XXX